Role of angular momentum in the production of complex fragments in fusion and quasifission reactions

Sh. A. Kalandarov,[1,2] G. G. Adamian,[1,2] N. V. Antonenko,[1] and W. Scheid[3]

[1]*Joint Institute for Nuclear Research, RU-141980 Dubna, Russia*
[2]*Institute of Nuclear Physics, 702132 Tashkent, Uzbekistan*
[3]*Institut für Theoretische Physik der Justus-Liebig-Universität, DE-35392 Giessen, Germany*

The influence of angular momentum on the competition between complete fusion followed by the decay of compound nucleus and quasifission channels is treated within the dinuclear system model. The charge distributions of the products in the reactions ^{28}Si+^{96}Zr, ^{4}He+^{130}Te, and ^{40}Ca+^{82}Kr are predicted at bombarding energies above the Coulomb barrier. The results of calculations for the reactions ^{93}Nb+^{9}Be,^{12}C,^{27}Al; ^{84}Kr+^{27}Al; ^{86}Kr+^{63}Cu; ^{139}La+^{12}C,^{27}Al; and ^{45}Sc+^{65}Cu are compared with the available experimental data.

I. INTRODUCTION

The rotational degree of freedom plays an important role in the capture and quasifission processes, the formation of a compound nucleus (CN), and the competition of decay channels in the excited CN. The nuclear reaction mechanism at low bombarding energies is assumed to be determined rather uniquely by the impact parameter or the angular momentum. The experimental evidence of the strong effect of angular momentum on the charge distribution of the complex fragments ($Z > 3$) is found out in Ref. [1]. As shown there, by measuring the final fragment spin distributions, one can extract information on the primary partial wave distributions contributing to the exit channels. Knowledge about the angular momentum dependence of the probability of the complex fragment emission is very important because of the increasing interest in the production of exotic nuclei via the cluster decay of the CN [2–6].

There are different models [7–15] for describing the complex fragment emission. The code GEMINI [14,15] treats the sequential statistical evaporation and binary decay of a hot CN and makes a sharp distinction between the decay widths for the emission of light particles and those for the emission of complex fragments. The widths for the emission of light particles are calculated using the Hauser-Feshbach approach with the sharp cutoff transmission coefficients. The complex fragment emission width is treated within the generalized transition state concept proposed in Ref. [16]. The rotating finite-range model [17] or the rotating liquid-drop model is used to calculate the conditional barriers for binary division. As found, the mass asymmetric fission barriers extracted from the experimental excitation functions lie between the values calculated with these two models [18,19]. Applications of the statistical model [14,15] are restricted to compound nucleus formation, and for a good description of the mass distribution with this model, the maximum angular momentum J_{max} of the system is specially adjusted.

The purpose of present work is to demonstrate the influence of angular momentum on the reaction mechanism and, correspondingly, on the charge and mass distributions of the reaction products. The detailed theoretical study of the reactions ^{93}Nb+^{9}Be, ^{45}Sc+^{65}Cu, ^{28}Si+^{96}Zr, ^{4}He+^{130}Te, and ^{40}Ca+^{82}Kr at low bombarding energies will be carried out within the dinuclear system (DNS) model [6]. In this model, cluster emission is treated under the assumption that the light clusters are produced by a collective motion of the nuclear system in the charge asymmetry coordinate with further thermal escape over the Coulomb barrier. The emission barriers for complex fragments are calculated within the DNS model by using the double-folding procedure (with the Skyrme-type density-depending effective nucleon-nucleon interaction) for the nuclear part of the nucleus-nucleus interaction potential. Both evaporation and binary decay are treated in the same way. The correct definition of the emission barriers and of their dependence on the angular momentum allows us to calculate the charge, mass, and kinetic energy distributions of the emitted complex fragments. The main ingredient of our description is the sophisticated potential energy as a function of angular momentum. The difference with respect to the statistical model [14,15] is a more accurate definition of the emission barriers. In our case, J_{max} is not an adjustable parameter, and it is calculated within our model by using the nucleus-nucleus interaction potential [6]. The dynamics plays a role at high angular momenta when quasifission becomes important. This clearly influences the yield of fission-like fragments. Note that the high J have larger contributions to the cross section. To test the model description, the calculated results will be compared with available experimental data.

II. MODEL

The DNS model [6,20] describes an evolution of the charge and mass asymmetry degrees of freedom, which are defined here by the charge and mass (neutron) numbers $Z = Z_1$ and $A = A_1$ ($N = N_1 = A - Z$) of the light nucleus of the DNS, in the DNS formed in the entrance channel of the reaction after the dissipation of the kinetic energy and angular momentum of relative motion. According to this description, there are nucleon drift and nucleon diffusion between the DNS nuclei, and eventually either a compound nucleus (CN) is formed (the complete fusion) or the DNS with given Z and A is formed

and decays (quasifission). After the formation, the excited CN decays by various channels including the formation of certain DNS and their decay. CN formation and its consequent decay are not necessarily the ultimate results of the evolution of the initial DNS. In addition to contributions from CN decay, the binary decay component is related to the quasifission mechanism. The competition between complete fusion and quasifission depends on the value of the maximum angular momentum deposited in the system. The quasifission and CN decays are hardly distinguished in the experiments, because in both cases two fragments are produced by the decay of the DNS formed during the diffusion process in the mass (charge) asymmetry coordinate with and without the stage of CN formation.

The cross section of the binary decay is calculated as follows [6]:

$$\sigma_{Z,A}(E_{\text{c.m.}}) = \sum_{J=0}^{J_{\max}} \sigma_{Z,A}(E_{\text{c.m.}}, J)$$

$$= \sum_{J=0}^{J_{\max}} \sigma_{\text{cap}}(E_{\text{c.m.}}, J) W_{Z,A}(E_{\text{CN}}^*, J), \quad (1)$$

where σ_{cap} is the partial capture cross section which defines the transition of the colliding nuclei over the Coulomb barrier and the formation of the initial DNS when the kinetic energy $E_{\text{c.m.}}$ and angular momentum J of the relative motion are transformed into the excitation energy and angular momentum of the DNS. The transition probability is calculated with the Hill-Wheeler formula. The value of $W_{Z,A}(E_{\text{CN}}^*, J)$ is the formation-decay probability of the DNS with the given asymmetries Z and A. The probability of the DNS formation is calculated statistically by using the stationary solution of the master equation with respect to the charge and mass asymmetries and depends on the potential energy of the DNS configurations at touching distance and on the thermodynamical temperature. The probability of the DNS decay in the R coordinate is calculated by using the transition state method. This probability depends on the difference between the potential energies of the DNS configurations at the touching distance and at the barrier position. The maximum value of angular momentum $J_{\max}$ is limited by either the kinematical angular momentum $J_{\text{kin}} = \{2\mu[E_{\text{c.m.}} - V(R_b)]/\hbar^2\}^{1/2} R_b$ [where R_b is the position of the Coulomb barrier with the height $V(R_b)$ and μ is the reduced mass] or by the critical angular momentum J_{cr} depending on which one is smaller: $J_{\max} = \min[J_{\text{kin}}, J_{\text{cr}}]$. The details of calculations of σ_{cap}, $W_{Z,A}(E_{\text{CN}}^*, J)$, and, correspondingly, $\sigma_{Z,A}(E_{\text{c.m.}})$ are given in Ref. [6]. Here, only the most salient features are outlined.

The DNS model describes the evolution of interacting nuclei along the following degrees of freedom: the relative distance R between the center of the nuclei; and the charge- and mass-asymmetry degrees of freedom, which are defined here by the charge Z and mass A of the light partner of the DNS. After the dissipation of kinetic energy and angular momentum of the relative motion, the DNS is trapped in the pocket of the interaction potential between partners. Then, a statistical equilibrium is reached in the mass-asymmetry coordinate so that the formation probability $P_{Z,A}$ of each DNS or CN configuration

depends on the potential energy $U(R_m, Z, A, J)$, calculated with respect to the potential energy of the rotational CN where R_m is the location of the minimum of the pocket in the nucleus-nucleus interaction potential. After the capture stage, there are nucleon drift and nucleon diffusion between the nuclei which constitute the DNS. Then, the excited DNS can decay with a probability $P_{Z,A}^R$ in the R coordinate if the local excitation energy of the DNS is high enough to overcome the barrier in the nucleus-nucleus potential. Ultimately, the system evolves either toward a CN configuration that subsequently decays, or to a DNS configuration. The latter process, in which a two-body configuration is kept along the trajectory, is the quasifission phenomenon.

The emission probability $W_{Z,A}(E_{\text{CN}}^*, J)$ of a fragment (Z, A) is calculated as the product of the DNS formation probability and the DNS decay probability:

$$W_{Z,A}(E_{\text{CN}}^*, J) = \frac{P_{Z,A} P_{Z,A}^R}{\sum_{Z',A'} P_{Z',A'} P_{Z',A'}^R}, \quad (2)$$

where the indices Z' and A' go over all possible channels from neutron evaporation to symmetric splitting. The probability $P_{Z,A}$ is the equilibrium limit of the master equation (see Ref. [6] for details) given by

$$P_{Z,A}(E_{\text{CN}}^*, J) \sim \exp[-U(R_m, Z, A, J)/T_{\text{CN}}(J)]. \quad (3)$$

Here, the n, p, d, and t evaporation channels are taken into consideration with $U(R_m, Z, A, J) = 0$. The quasifission barrier B_R^{qf}, calculated as the difference between the bottom of the inner pocket and the top of the external barrier, prevents the decay of the DNS along the R degree of freedom with the weight $P_{Z,A}^R$ given as

$$P_{Z,A}^R \sim \exp\left[-B_R^{\text{qf}}(Z, A, J)/T_{Z,A}(J)\right]. \quad (4)$$

In Eqs. (3) and (4), $T_{\text{CN}}(J)$ and $T_{Z,A}(J)$ are the temperatures of the CN and DNS, respectively. For the emission of particles with $Z < 2$, $T_{Z,A}(J) = T_{\text{CN}}(J)$ and $B_R^{\text{qf}}(Z, A, J)$ is equal to the particle binding energy plus the value of the Coulomb barrier at $Z \neq 0$. The Fermi-gas model is employed to compute the temperature, with a level-density parameter $a = 0.114A + 0.162A^{2/3}$.

In the calculations, we use formulas (1) and (2) to treat the sequential statistical decay (the evaporation of light particles and/or the binary decay) of the hot system. The generation of the whole cascade of decay channels is performed by the Monte Carlo method. We continue to trace the decay processes until all fragments become cold (the excitation energy of fragments is smaller than its neutron emission threshold). The number n of generation of events in the Monte Carlo technique was chosen according to the smallest decay probability which is $\sim 1/n$. Number $n > 10^4$ of iterations is large enough to obtain the calculated results with a high accuracy.

III. RESULTS OF CALCULATIONS

To test our method, we treated the charge distributions of the emitted complex clusters for the reactions ^{93}Nb+^{9}Be at $E_{\text{lab}} = 8.4$, 11.4, and 18 MeV/nucleon; ^{93}Nb+^{12}C at $E_{\text{lab}} = 11.4$ and 18; ^{93}Nb+^{27}Al at $E_{\text{lab}} = 11.4$ and 18 (Fig. 1);
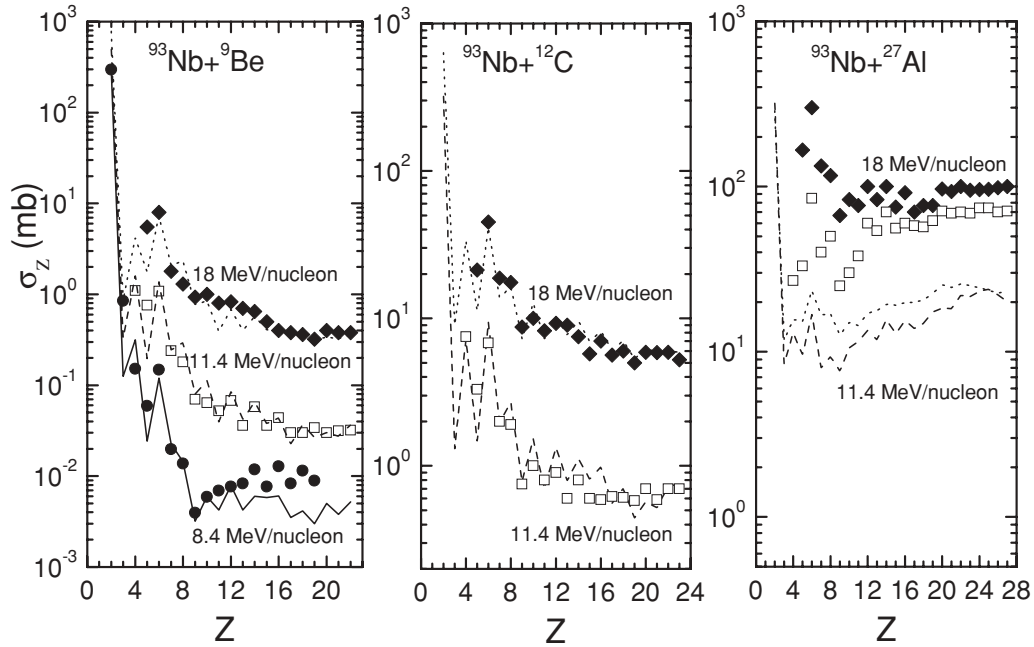
FIG. 1. Calculated charge distributions (lines) of the products in the reactions ^{93}Nb+^{9}Be,^{12}C,^{27}Al at the indicated bombarding energies. The experimental data [14] are shown by the symbols.

^{84}Kr+^{27}Al at $E_{lab} = 5.9$ and 10.6; ^{86}Kr+^{63}Cu at $E_{lab} = 5.65$, 6.4, and 7.44 (Fig. 2); ^{139}La+^{12}C at $E_{lab} = 14.7$ and 18; ^{139}La+^{27}Al at $E_{lab} = 14.7$ and 18 (Fig. 3); and ^{45}Sc+^{65}Cu at $E_{lab} = 4.44$ MeV/nucleon (Fig. 4). In Figs. 1–4, the calculated cross sections

$$\sigma_Z(E_{c.m.}) = \sum_A \sigma_{Z,A}(E_{c.m.}) \qquad (5)$$

are in a good agreement with the experimental data [1,14,21–23] for the asymmetric and almost symmetric reactions excepting the ^{93}Nb+^{27}Al reaction. One can well reproduce the relative yields of different products but not the magnitude of the experimental σ_Z [14]. To describe the experimental data for this reaction, we should assume unrealistically large maximum angular momentum, $J_{max} = 110$ at $E_{lab} = 11.4$ MeV/nucleon and $J_{max} = 132$ at
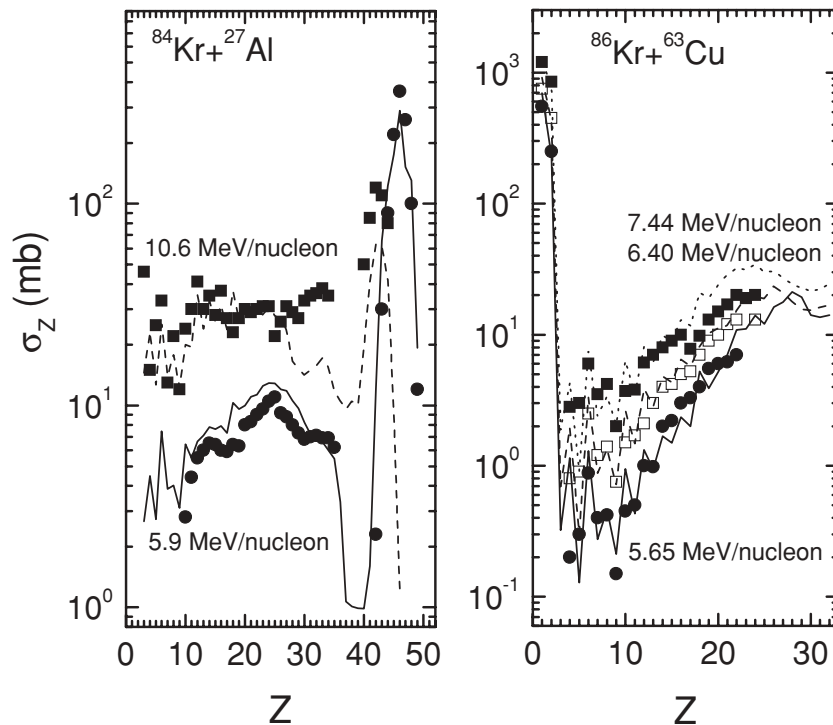

FIG. 2. Calculated charge distributions (lines) of the products in the reactions ^{84}Kr+^{27}Al and ^{86}Kr+^{63}Cu at the indicated bombarding energies. The experimental data [21,22] are shown by the symbols.
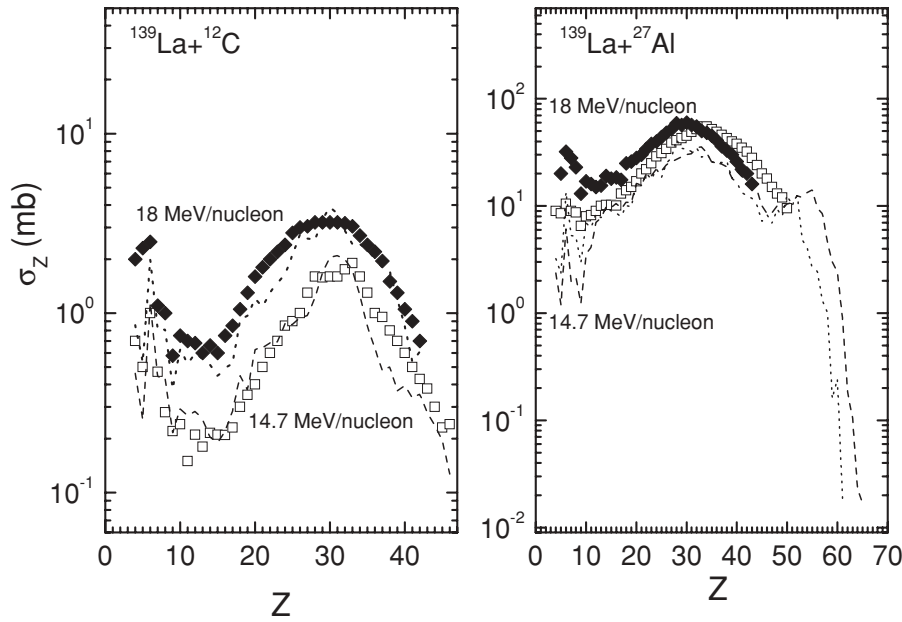
FIG. 3. Calculated charge distributions (lines) of the products in the reactions ^{139}La+^{12}C,^{27}Al at the indicated bombarding energies. The experimental data [23] are shown by the squares.

$E_{lab} = 18$ MeV/nucleon. In our calculations, $J_{max} = 66$ for both energies. We cannot explain why the experimental cross sections for the ^{93}Nb+^{27}Al reaction are about 4 times larger than those for the similar reaction ^{84}Kr+^{27}Al and why the cross sections of the almost symmetric fragmentations in the ^{93}Nb+^{27}Al reaction are much larger than those for the ^{139}La+^{27}Al reaction.

To study the influence of angular momentum on the reaction mechanism, we consider the reactions ^{93}Nb+^{9}Be
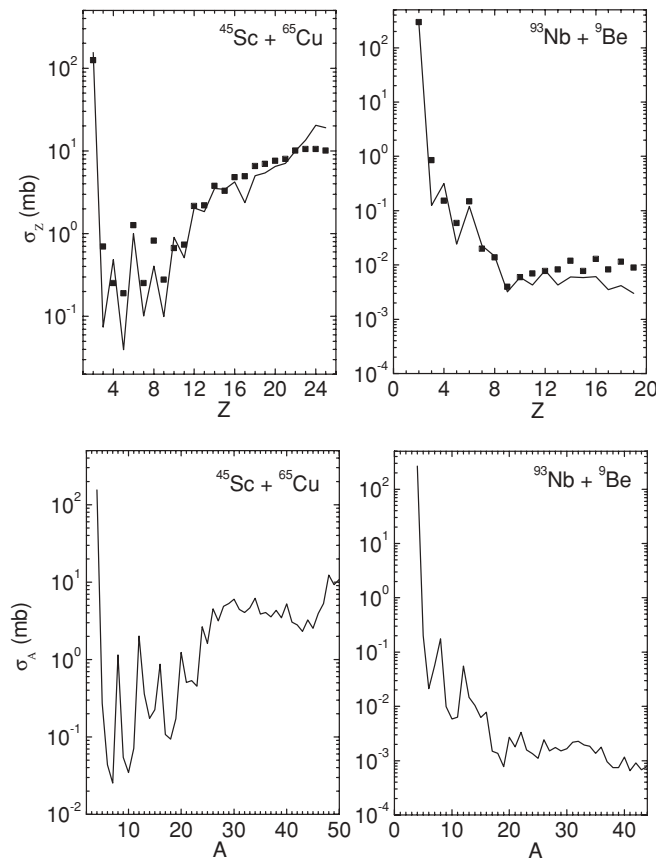

FIG. 4. Calculated charge (upper) and mass (lower) distributions of the products in the reactions ^{93}Nb($E_{lab} = 8.4$ MeV/nucleon)+^{9}Be and ^{45}Sc(E_{lab}=4.44 MeV/nucleon)+^{65}Cu. The experimental data [1] are shown by the solid squares.
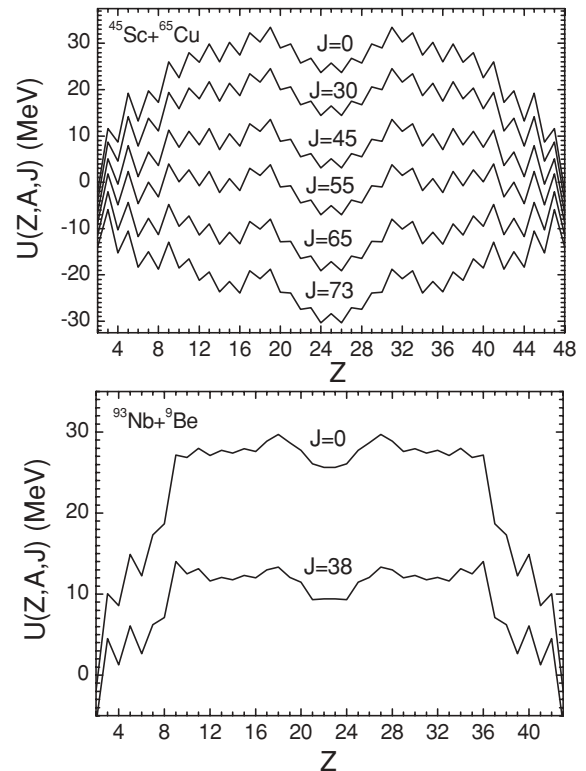

FIG. 5. Driving potentials at different angular momenta for the systems ^{93}Nb+^{9}Be (lower) and ^{45}Sc+^{65}Cu (upper). The value of U is normalized to the energy of the rotating CN.
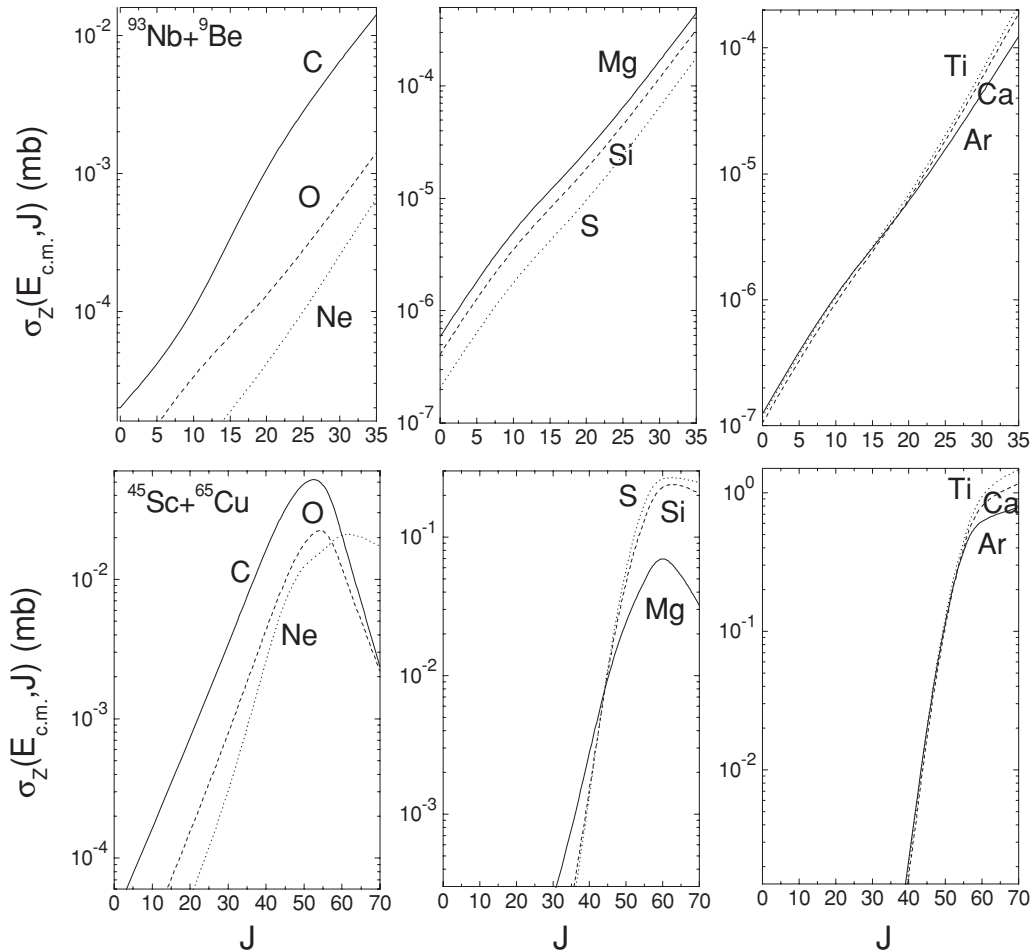
FIG. 6. Calculated partial production cross sections for the indicated nuclei in the reactions ^{93}Nb(E_{lab}=8.4 MeV/nucleon)+^{9}Be (upper) and ^{45}Sc(E_{lab}=4.44 MeV/nucleon)+^{65}Cu (lower).

at $E_{lab} = 8.4$ MeV/nucleon and ^{45}Sc+^{65}Cu at $E_{lab} = 4.44$ MeV/nucleon leading to the CN ^{102}Rh [$E^*_{CN}(J = 0) = 80$ MeV, $J_{max} = J_{cr} = 38$] and ^{110}Sn [$E^*_{CN}(J = 0) = 95.6$ MeV, $J_{max} = J_{kin} = 73$], respectively. The potential energies $U(Z, A, J)$ [6] of the DNS versus Z are presented in Fig. 5 at different values of J for these reactions. Because the mode responsible for the N/Z equilibrium in the DNS is the fast one, the potential energies U are minimized with respect to the mass asymmetry for each fixed charge asymmetry. Note that the driving potential U is sensitive to the total mass number of the DNS. Comparing the driving potentials for these reactions, one can conclude that the odd-even staggering decreases with increasing N/Z ratio in the system (Fig. 5). One can observe the strong angular momentum dependence of the driving potential which governs the reaction mechanism. For ^{45}Sc+^{65}Cu, the CN configuration seems to be energetically more favorable than any DNS configuration at $J < J_0 = 50 \leqslant J_{max}$ (Fig. 5). There is no hindrance for the complete fusion in this case. Because the CN is produced with larger excitation energy, the fusion yield appears as the evaporation residues and the binary decay products. The evaporation residues are the dominant fusion products in this reaction. For higher partial

waves $J_0 = 50 \leqslant J \leqslant J_{max}$, the calculated driving potentials show global minimum at the symmetric DNS but not at the CN configuration (the potential energy U of DNS, normalized to the energy of rotating CN, is negative). It is clear that the charge (mass) drift pushes the system toward symmetry. This indicates that complete fusion becomes energetically denied and higher J waves do not lead to fusion, but to the quasifission resulting in the fragments produced as the binary decay products of the transient DNS originating from the target-projectile DNS. This implies that at higher partial waves, most of the heavy complex fragments are produced by quasifission. For ^{45}Sc+^{65}Cu, at $J_0 = 50$, the CN and symmetric DNS potential energies coincide, and we can observe the coexistence of the quasifission and fusion-decay events. Thus, at the value of J_0 the reaction mechanisms become less clear-cut. For the ^{93}Nb+^{9}Be reaction, the driving potential is positive at $J \leqslant J_{max}$, which means that the decay products are mainly from the decay of the excited CN.

We treated the charge distributions of the emitted complex fragments in the reactions ^{93}Nb(8.4 MeV/nucleon)+^{9}Be and ^{45}Sc(4.44 MeV/nucleon)+^{65}Cu (Fig. 4). In Ref. [1] the differential cross sections $d\sigma_Z/d\Omega$ are presented at

$\theta_{\rm c.m.} = 90^{\rm o}$. To obtain total cross section, one can assume with a good accuracy that the angular distribution is $1/\sin(\theta_{\rm c.m.})$ [1]. In this case the data of Ref. [1] are multiplied by a factor of $2\pi^2$. Note that angular momentum influences the angular distribution, increasing the anisotropy. However, the restored total cross section (the integral value) would vary within 10% if we took the angular momentum into account in the angular distribution. In Fig. 4, the calculated cross sections $\sigma_Z(E_{\rm c.m.})$ are in a good agreement with the experimental data [1]. These charge distributions are completely different because the complex fragments are produced mostly by quasifission in the ^{45}Sc+^{65}Cu reaction and by complex fragment emission from the excited CN in the ^{93}Nb+^{9}Be reaction. As found, the relative contributions from high-partial waves to the yields of the complex fragments are considerable. The experimental maxima of the charge distributions are correctly reproduced. The odd-even effects are visible in the charge distributions for light fragments. This fact indicates the influence of shell structure of the DNS nuclei on the evolution and decay of the system. The odd-even effects become weaker for larger values of Z. The average excitation energies and spins of the primary light products are rather small. For light nuclei with $Z \lesssim 10$, the excitation energy is below the neutron emission threshold, and these nuclei do not decay further. For binary decay with $Z > 10$, the fragments have the average excitation energy and spin of about 10–30 MeV and 3–8, respectively. These primary products decay solely by light-particle (n, p, α) emission (for example, the products extends down to lower Z values and the secondary Z distribution is removed from the primary one) resulting in evaporation residues. Thus, the odd-even structures of the charge distributions are washed out due to the sequential evaporation.

The dependencies of the partial cross section

$$\sigma_Z(E_{\rm c.m.}, J) = \sum_A \sigma_{Z,A}(E_{\rm c.m.}, J) \qquad (6)$$

on the angular momentum J for the even-Z complex fragments are presented in Fig. 6. For the ^{45}Sc+^{65}Cu reaction, most of the (C, O), (Ne, Mg, Si, S), and (Ar, Ca, Ti) yields come from angular momenta around $J \approx 50$–55, $J \approx 60$–65, and $J \approx J_{\rm max}$. All binary decays with these fragments have both CN and quasifission origins. Most of these fragments are produced at J between J_0 and $J_{\rm max}$. This indicates again that quasifission is the dominant production mechanism for a heavy complex fragment. Let us compare in more detail the decays with C and Mg. At $J \approx J_0$, the yields of these fragments are almost the same. With increasing angular momentum from about J_0 up to $J_{\rm max}$ the yield of C decreases but the yield of Mg increases. The reason is that the difference of the potential energies of the DNS with the C nucleus and of the DNS with the Mg nucleus decreases with increasing J (Fig. 5) because of the difference of the moments of inertia of these configurations. At $J = 0$ ($J = J_{\rm max}$) the DNS with C nucleus is the energetically more favorable (unfavorable) configuration than the DNS with Mg nucleus. At $J \approx J_0$, the potential energies of these configurations become equal to each other. Thus, the angular momentum strongly influences the competition between the binary decay channels and, correspondingly, the probability of
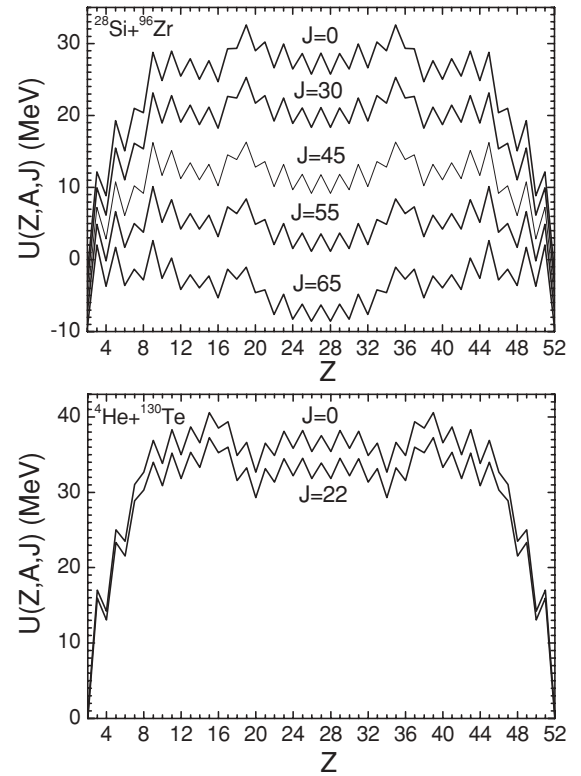

FIG. 7. Same as in Fig. 5, but for the systems ^{28}Si+^{96}Zr (upper) and ^{4}He+^{130}Te (lower).

complex fragment emission. The reaction mechanism (fusion decay and quasifission) is mostly determined by the maximum angular momentum deposited in the initial DNS. The emission from the excited CN in the ^{93}Nb+^{9}Be reaction provides other dependencies of σ_Z on J (Fig. 6).

For the ^{28}Si(5.7 MeV/nucleon)+^{96}Zr and ^{4}He (26 MeV/nucleon)+^{130}Te reactions, $J_{\rm max} = J_{\rm cr} = 68$ and $J_{\rm max} = J_{\rm cr} = 22$, respectively, and the excitation energies of the CN ^{124,134}Xe formed are the same, $E_{\rm CN}^*(J = 0) = 104$ MeV. For the ^{28}Si+^{96}Zr system, at $J_0 = 57$ the CN and symmetric DNS potential energies coincide (Fig. 7). Since $J_0 < J_{\rm max}$ ($J_0 > J_{\rm max}$) for the ^{28}Si+^{96}Zr (^{4}He+^{130}Te) reaction, the quasifission (complete fusion) channel becomes dominant among the competing channels. As a result, the charge distributions in these two reactions strongly differ (Fig. 8). The symmetric binary decay channel in the ^{28}Si+^{96}Zr reaction is not so strongly dominant as in the case of the ^{45}Sc+^{65}Cu reaction. To understand this difference, one can see in Figs. 5 and 7 that the driving potential for the ^{45}Sc+^{65}Cu system has a deeper minimum at the symmetry.

The calculated charge distributions for the ^{40}Ca+^{82}Kr reaction at $E_{\rm lab} = 3.6$ MeV/nucleon [$E_{\rm CN}^*(J = 0) = 55$ MeV, $J_{\rm max} = J_{\rm kin} = 32$] and $E_{\rm lab} = 5.5$ MeV/nucleon [$E_{\rm CN}^*(J = 0) = 105$ MeV, $J_{\rm max} = J_{\rm cr} = 75$] leading to the CN ^{122}Ba are shown in Fig. 9. Since for both bombarding energies, different maximum angular momenta are involved and $J_0 = 49$, the charge distributions are strongly different. The calculated values of σ_Z at 5.5 MeV/nucleon are in a good agreement
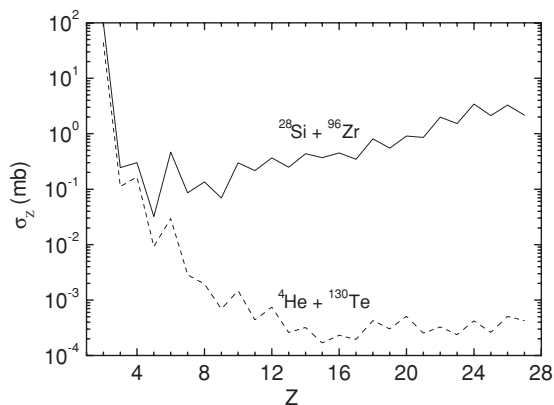
FIG. 8. Predicted charge distributions of products in the reactions ^{28}Si($E_{\text{lab}} = 5.7$ MeV/nucleon)$+^{96}$Zr (solid line) and ^{4}He($E_{\text{lab}} = 26$ MeV/nucleon)$+^{130}$Te (dashed line).

with the experimental data [5]. Again the odd-even staggering is well pronounced for Z <8. At smaller bombarding energy (smaller excitation) this staggering is visible also at larger Z. This means that the sequential emission from fragments is inhibited at smaller energy and the odd-even effects are not washed out.

IV. SUMMARY

The important role of the angular momentum of the system in the emission of complex fragments is demonstrated. The reaction mechanism (fusion followed by binary decay or quasifission) is mostly determined by the angular momentum deposited in the system. The value of the maximum angular momentum for a capture process can be controlled by either the projectile-target mass and charge asymmetries or by the kinetic
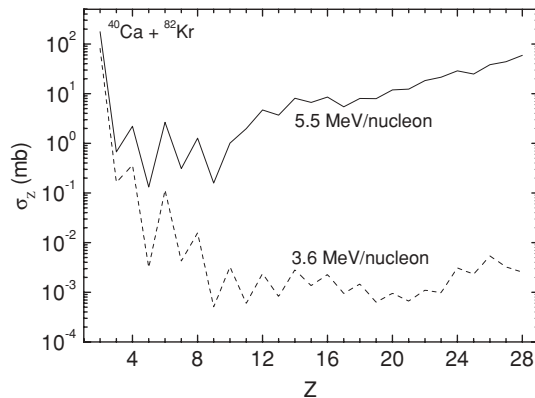

FIG. 9. Calculated charge distributions of products in the reaction ^{40}Ca$+^{82}$Kr at $E_{\text{lab}} = 3.6$ MeV/nucleon (dashed line) and at $E_{\text{lab}} = 5.5$ MeV/nucleon (solid line).

energy of projectile. At high angular momenta, the complex fragments and the fission-like fragments in the reactions ^{45}Sc$+^{65}$Cu, ^{28}Si$+^{96}$Zr, and ^{40}Ca$+^{82}$Kr mainly originate from the quasifission process. The average time for emission or quasifission is longer than the rotation period of the dinuclear system. So, the angular distributions are well approximated by $1/\sin(\theta_{\text{c.m.}})$. The complete fusion followed by binary decay is dominant in the reactions ^{93}Nb$+^{9}$Be and ^{4}He$+^{130}$Te at low angular momenta.

[1] L. G. Sobotka *et al.*, Phys. Rev. C **36**, 2713 (1987); L. G. Sobotka (private communication).

[2] J. G. del Campo *et al.*, Phys. Rev. C **57**, R457 (1998).

[3] M. La Commara *et al.*, Nucl. Phys. A **669**, 43 (2000).

[4] J. Töke, J. Lu, and W.-U. Schröder, Phys. Rev. C **67**, 034609 (2003); B. Djerroud *et al.*, *ibid.* **64**, 034603 (2001); J. Töke, D. K. Agnihotri, W. Skulski, and W.-U. Schröder, *ibid.* **63**, 024604 (2001).

[5] J.-P. Wieleczko *et al.*, Acta Phys. Pol. B **40**, 577 (2009); in *Proceeding of the International Conference on Nuclear Structure and Related Topics* (JINR, Dubna, 2009), p. 236; G. Ademard and J.-P. Wieleczko *et al.*, Phys. Rev. C (in print).

[6] Sh. A. Kalandarov, G. G. Adamian, N. V. Antonenko, and W. Scheid, Phys. Rev. C **82**, 044603 (2010).

[7] W. A. Friedman and W. G. Lynch, Phys. Rev. C **28**, 16 (1983).

[8] R. G. Stokstad, in *Treatise on Heavy Ion Science*, edited by D. A. Bromley (Plenum, New York, 1984), Vol. III.

[9] A. J. Cole, *Statistical Models for Nuclear Decay* (IOP Publishing, Bristol, UK, 2000).

[10] J. G. Gomez del Campo, J. L. Charvet, A. D'Onofrio, R. L. Auble, J. R. Beene, M. L. Halbert, and H. J. Kim, Phys. Rev. Lett. **61**, 290 (1988); J. G. Gomez del Campo, R. L. Auble, J. R. Beene, M. L. Halbert, H. J. Kim, A. D'Onofrio, and J. L. Charvet, Phys. Rev. C **43**, 2689 (1991).

[11] T. Matsuse, C. Beck, R. Nouicer, and D. Mahboub, Phys. Rev. C **55**, 1380 (1997).

[12] F. Auger, B. Berthier, A. Cunsolo, A. Foti, W. Mittig, J. M. Pascaud, E. Plagnol, J. Québert, and J. P. Wieleczko, Phys. Rev. C **35**, 190 (1987).

[13] R. K. Gupta, M. Balasubramaniam, C. Mazzocchi, M. La Commara, and W. Scheid, Phys. Rev. C **65**, 024601 (2002); R. Kumar and R. K. Gupta, *ibid.* **79**, 034602 (2009).

[14] R. J. Charity *et al.*, Nucl. Phys. A **483**, 371 (1988).

[15] R. J. Charity *et al.*, Nucl. Phys. A **476**, 516 (1988).

[16] L. G. Moretto, Nucl. Phys. A **247**, 211 (1975); L. G. Moretto and G. J. Wozniak, Prog. Part. Nucl. Phys. **21**, 401 (1988).

[17] A. J. Sierk, Phys. Rev. Lett. **55**, 582 (1985).

[18] K. X. Jing *et al.*, Nucl. Phys. A **645**, 203 (1999).

[19] J. Boger and J. M. Alexander, Phys. Rev. C **50**, 1006 (1994).

[20] V. V. Volkov, Izv. Akad. Nauk SSSR, Ser. Fiz. **50**, 1879 (1986); G. G. Adamian, A. K. Nasirov, N. V. Antonenko, and R. V. Jolos, Phys. Part. Nuclei **25**, 583 (1994); G. G. Adamian, N. V. Antonenko, and W. Scheid, Nucl. Phys. A **618**, 176 (1997); G. G. Adamian, N. V. Antonenko, W. Scheid, and V. V. Volkov, *ibid.* **627**, 361 (1997); **633**, 409 (1998); G. G. Adamian, N. V. Antonenko, and W. Scheid, Phys. Rev. C **68**, 034601 (2003).

[21] W. F. W. Schneider *et al.*, Nucl. Phys. A **371**, 493 (1981); Y. Futami *et al.*, *ibid.* **607**, 85 (1996).

[22] J. Boger *et al.*, Phys. Rev. C **49**, 1597 (1994).

[23] R. J. Charity *et al.*, Nucl. Phys. A **511**, 59 (1990).